Two-Order Targeted Brain Tumor Imaging by Using an Optical/Paramagnetic Nanoprobe across the Blood Brain Barrier

Huihui Yan,[‡] Lu Wang,[†] Jiyao Wang,[‡] Xiaofu Weng,[§] Hao Lei,[⊥,*] Xuxia Wang,[⊥] Lu Jiang,[∥] Jianhua Zhu,[†] Weiyue Lu,[†] Xunbin Wei,[§,*] and Cong Li[†,*]

[†]Key Laboratory of Smart Drug Delivery, Ministry of Education & PLA, School of Pharmacy, Fudan University, Shanghai 201203, China, [‡]Department of Gastroenterology, Zhongshan Hospital affiliated with Fudan University, 180 Fenglin Road, Shanghai 200032, China, [§]Med-X Research Institute and School of Biomedical Engineering, Shanghai Jiao Tong University, Shanghai 200030, China, [⊥]State Key Laboratory of Magnetic Resonance and Atomic and Molecular Physics, Wuhan Institute of Physics & Mathematics, The Chinese Academy of Sciences, Wuhan 430071, China, and [∥]JHU ICMIC Program, The Russell H. Morgan Department of Radiology and Radiological Science, Johns Hopkins University School of Medicine, Baltimore, Maryland 21205, United States

ABSTRACT Surgical resection is a mainstay of brain tumor treatments. However, the completed excision of malignant brain tumor is challenged by its infiltrative nature. Contrast enhanced magnetic resonance imaging is widely used for defining brain tumor in clinic. However its ability in tumor visualization is hindered by the transient circulation lifetime, nontargeting specificity, and poor blood brain barrier (BBB) permeability of the commercially available MR contrast agents. In this work, we developed a two-order targeted nanoprobe in which MR/optical imaging reporters, tumor vasculature targeted cyclic [RGDyK] peptides, and BBB-permeable Angiopep-2 peptides are labeled on the PAMAM-G5 dendrimer. This nanoprobe is supposed to first target the $\alpha_v\beta_3$ integrin on tumor vasculatures. Increased local concentration of nanoprobe facilitates the association between BBB-permeable peptides and the low-density lipoprotein receptor-related protein (LRP) receptors on the vascular endothelial cells, which further accelerates BBB transverse of the nanoprobe *via* LRP receptor-mediated endocytosis. The nanoprobes that have penetrated the BBB secondly target the brain tumor because both $\alpha_v\beta_3$ integrin and LRP receptor are highly expressed on the tumor cells. *In vivo* imaging studies demonstrated that this nanoprobe not only efficiently crossed intact BBB in normal mice, but also precisely delineated the boundary of the orthotropic U87MG human glioblastoma xenograft with high target to background signal ratio. Overall, this two-order targeted nanoprobe holds the promise to noninvasively visualize brain tumors with uncompromised BBB and provides the possibility for real-time optical-image-guided brain tumor resection during surgery.

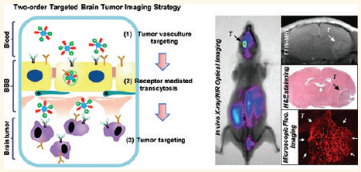

KEYWORDS: brain tumor · nanoprobe · multimodal imaging · blood brain barrier · two-order targeting

Even though the advances in tumor diagnosis and therapy have improved the survival of cancer patients, malignant brain tumors continue to be the cause of disproportionate morbidity and mortality.[1] For example, the median survival of patients suffering from aggressive glioblastoma multiforme (GBM) is about 15 months, and from anaplastic astrocytoma (AA), 2−3 years.[1,2] The standard therapy for brain tumors involves surgical resection followed by radiotherapy and/or chemotherapy.[3] However, malignant brain tumors are hard to eliminate completely due to their heterogeneous and infiltrative nature, which leads to the precise resection of tumor from the surrounding healthy brain tissue being difficult during surgery.[4] Magnetic resonance imaging (MRI) is a standard neuroimaging technique for preoperative localization of brain tumor.[5,6] Gadolinium (Gd^{3+})-based MR contrast agents (CAs) such as Gd^{3+}-DTPA (Magnevist) are widely used to define tumor margins in the clinic.[7] These small molecular MR CAs diffuse into the tumor bed, where the blood brain barrier (BBB) is disrupted, and lead to MR signal enhancement. Unfortunately, the Gd approach is limited in that about 10% GBM and 30% AA do not show any MR signal enhancement due to uncompromised BBB.[8] Moreover, the transient circulation lifetime and nontargeting specificity of these CAs further hinder their application. Therefore, probes with BBB permeability, optimized circulation lifetime, and high targeting specificity are needed.

Nanoprobes demonstrate advantages in tumor imaging including a tunable circulation lifetime,[9] enhanced permeability and retention (EPR) effect that up-regulates intratumoral delivery due to the high permeability of tumor vasculatures,[10,11] and multivalent effect that increases receptor targeting specificity by labeling multiple ligands on a single nanoparticle.[12] Even though previous works unambiguously showed the capability of nanoprobes to visualize subcutaneous tumor xenografts *in vivo*,[13,14] the performance of these nanoprobes for brain tumor imaging is far from satisfactory because the BBB prevents

* Address correspondence to congli@fudan.edu.cn; xwei01@sjtu.edu.cn; leihao@wipm.ac.cn.

Received for review September 30, 2011 and accepted December 10, 2011.

Published online December 11, 2011
10.1021/nn203749v

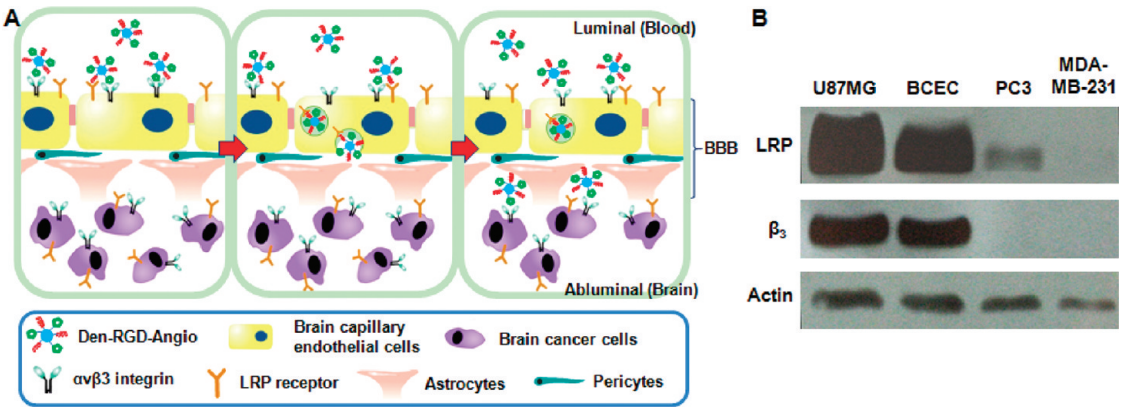

Figure 1. Design of the two-order targeted nanoprobe for brain tumor imaging. (A) Overview of two-order targeted brain tumor imaging strategy. The nanoprobe first targets the $\alpha_V\beta_3$ integrin on tumor vasculatures. After binding with nearby LRP receptors, the nanoprobe traverses BBB *via* LRP receptor-mediated transcytosis and finally targets tumor cells directly. (B) Western blot shows the overexpression of both $\alpha_V\beta_3$ integrin and LRP receptor in human gliomblastoma U87MG cancer cells and BCECs.

the intracerebral delivery of almost all exogenous macromolecules.[15] Receptor-mediated transcytosis is a natural pathway through which endogeneous proteins pass the BBB.[16] Receptors present on brain capillary endothelial cells (BCECs) play an active role in mediating the intracerebral delivery of their corresponding ligands. Taking advantage of this property, receptor targeting ligands such as transferrin (Tf),[17] rabies virus glycoprotein peptide (RVG29),[18] and snake neurotoxin candoxin peptide (CDX)[19] were functionalized into the nanoparticles to up-regulate their BBB permeability. Recently, Jia *et al*. reported a drug delivery vector in which two different receptor-targeting ligands, Tf and wheat germ agglutinin (WGA), were conjugated.[20] The improved therapeutic efficacy of this nanoparticle on brain tumor was explained by the increased intratumoral delivery of the chemotherapeutics resulting from the synergistic effect of Tf-associated receptor-mediated transcytosis and WGA-associated adsorptive endocytosis. The above work demonstrated the feasibility to enhance the brain tumor uptake of nanoparticles by increasing their BBB traverse efficiency.

In this work, we developed a novel two-order targeted imaging strategy, which visualizes brain tumor by up-regulating the BBB permeability and receptor targeting specificity of nanoprobes (Figure 1A). In this strategy, a nanoparticle labeled with MR/optical imaging reporters, tumor vasculature targeting cyclic [RGDyK] peptides, and BBB-permeable Angiopep-2 peptides was prepared. In the first step, this nanoprobe targets the tumor neovasculatures that are abundant in the tumor periphery. The increased local concentration of the nanoprobe facilitates the association between the BBB-permeable peptide and the corresponding receptor on the vascular endothelial cells, which accelerates BBB transverse of the nanoprobe *via* receptor-mediated transcytosis. In the second step, the nanoprobes that have penetrated the BBB target the brain tumor directly because the corresponding receptors are also highly expressed on tumor cells. This two-order targeting strategy realizes the specific intratumoral delivery of imaging probes without disturbing the normal function of the BBB. $\alpha_V\beta_3$ integrin as a receptor for extracellular matrix proteins is overexpressed on the activated endothelial cells of tumor neovasculatures, certain tumor cells, but not the normal vasculatures.[21] Therefore, $\alpha_V\beta_3$ integrin presents an ideal molecular target for tumor diagnosis and therapy.[22] The cyclic arginine-glycine-aspartic (RGD) tripeptide sequence shows higher binding affinity to $\alpha_V\beta_3$ integrin (subnanomolar level),[23] and c[RGDyK] peptide was chosen as the tumor vasculature targeting ligand here due to its convenience in being labeled covalently on nanoparticles. Meanwhile, low-density lipoprotein receptor-related protein (LRP) plays an active role in mediating the transport of numerous ligands across the BBB including lipoproteins, protease/protease inhibitor complexes, and extracellular matrix proteins.[24,25] Angiopep-2, a 19 amino acid peptide derived from the common peptidic sequence of the LRP protein ligands, demonstrates a much higher BBB transcytosis efficacy than transferrin and its mother molecule aprotinin.[26,27] Importantly, LRP receptors are expressed not only in BCECs, but also in many types of glioblastomas.[28] Therefore, angiopep-2 was chosen as the BBB-permeable ligand functionalized on the nanoprobe.

Like a "Great Wall" in the brain, the BBB protects the brain microenvironment from fluctuations in concentrations of ions, metabolites, and unwanted materials in the circulation system and keeps the brain working under perfect conditions.[29] However, this defense proves to be a nightmare during the treatment of brain tumor or other neurological diseases.[30,31] Therefore, the intracerebral delivery of imaging/therapeutic agents by circumventing the BBB is a challenging but meaningful task. The objective of this work is to

evaluate a novel imaging strategy to noninvasively visualize the brain tumor with high sensitivity and target the background signal ratio without compromising the BBB.

RESULTS

Receptor Expression Level on Targeted Cells. High expression of both $\alpha_V\beta_3$ integrin and LRP receptor in BCECs and brain cancer cells is a prerequisite for the success of the two-order targeted imaging strategy. Receptor expression levels in the targeted cells were immunoblotted by LRP1 and β_3 antibodies, respectively. As shown in Figure 1B, BCECs demonstrated immunoreactive bands at 85 and 110 kDa, the anticipated molecular weights of LRP receptor and $\alpha_V\beta_3$ integrin. The receptor expression levels were also tested in three human cancer cell lines including glioblastoma U87MG cells, prostate PC3 cells, and breast MDA-MB-231 cells. U87MG cells demonstrated the highest expression level of LRP receptor. Densitometry studies showed that LRP receptor levels in U87MG and BCECs were much higher than those in PC3 and MDA-MB-231 cells. Meanwhile, U87MG and BCEC cells showed a comparable β_3 integrin expression level, but this receptor was not found in PC3 and MDA-MB-231 cells.

Design, Synthesis, and Characterization of the Nanoprobes. The fifth generation (G5) PAMAM dendrimer was chosen as a platform of the nanoprobes due to its globular architecture, identical molecular weight, optimized circulation lifetime, and well-defined reactive groups on the particle surface.[32,33] Near-infrared (NIR) fluorophore Cy5.5 was labeled on the dendrimer because tissue absorption and autofluorescence in this region (650−900 nm) are low, which allows the NIR light to penetrate deep tissue.[34] Conjugated rhodamine was used to track the nanoprobes in either cells or excised tissues because Cy5.5 cannot be excited well under a conventional fluorescent microscope. Gd^{3+}-DOTA was chosen as the MR CAs functionalized on the nanoprobe due to its high thermodynamic stability and kinetic inertness.[35] Both angiopep-2 and c[RGDyK] peptides were labeled on the dendrimer through a PEG linker. This extended PEG linker not only improves the biocompatibility of the nanoprobe but also minimizes the steric hindrance of the hyperbranched polymer to the targeting specificity of ligands.

The targeted nanoprobe **Den-RGD-Angio** labeled with both angiopep-2 and c[RGDyK] peptides and the control nanoprobes **Den-RGD** modified with only c[RGDyK] peptides were synthesized in Figure 2A. Briefly, treatment of maleimide (Mal) and *N*-hydroxysuccinimidyl (NHS) ester-functionalized PEG derivative Mal-PEG^{2k}-NHS with c[RGDyK] offered compound **1**, which further reacted with dendrimer to give **2**. The conjugation of NHS esters of rhodamine, Cy5.5, and DOTA with **2**, respectively, gave **3**, which then complexed with Gd^{3+} ions to produce **Den-RGD**. The reaction between bis-functionalized PEG derivative Mal-PEG^{2k}-NH_2 and *N*-succinimidyl 3-(2-pyridyldithio)propionate (SPDP) gave **4**. The condensation between **4** and **2** resulted in **5**. The conjugation of NHS esters of rhodamine, Cy5.5, and DOTA with **5** subsequently gave **6**, which further reacted with peptide TFFYGGSRGKRNNFKTEEYC followed by a complexation with Gd^{3+}, yielding **Den-RGD-Angio**. The detailed synthetic procedure of **Den-RGD** and **Den-RGD-Angio** is described in the Supporting Information. Meanwhile, the synthesis of control nanoprobes **Den-Angio** labeled with angiopep-2 peptides and **Den-PEG** without any targeting ligand is described in our previous work.[36] The chemical structures of four nanoprobes are presented in Figure 2B.

The physical parameters of these nanoprobes are listed in Table 1. The hydrodynamic diameter of **Den-RGD-Angio** was determined as 15.6 nm, which was slightly larger than that of control nanoprobes. The polydispersity index (PDI) of all nanoprobes stayed below 0.3, and every nanoprobe migrated as a single band in the fluorescence images of the resolved sodium dodecyl sulfate-polyacrylamide gel electrophoresis (SDS-PAGE) (Figure S1). All nanoprobes showed positive charges in physiological pH, but the values were much lower than that of unconjugated G5 dendrimer (Figure S2). The molar ratio of angiopep-2/c[RGDyK]/Gd^{3+}-DOTA/dendrimer in **Den-RGD-Angio** was measured as 5/6/54/1. The molecular weights (MWs) of these nanoprobes were determined by MALDI-TOF mass spectra (Figure S3). All nanoprobes demonstrated similar longitudinal relaxivity r_{1p} values in a range 7.1−7.4 mM^{-1} s^{-1}/Gd^{3+}.

Cytotoxicity and Cellular Uptake Studies. The cytotoxicities of the nanoprobes were evaluated in U87MG cells *via* MTT assay. As shown in Figure S4, all nanoprobes demonstrated much lower cytotoxicities compared to the unmodified dendrimer. The IC_{50} values of the nanoprobes were measured in the range 6−30 μM and were at least 20 times higher than that of unmodified dendrimer (0.3 μM). *In vitro* confocal fluorescence microscopic imaging demonstrated the attachment of **Den-RGD-Angio** on the cell membrane when the U87MG cells were treated with this nanoprobe for 15 min at 4 °C (Figure 3A). Above experiment verifies the ligand/receptor association because the active cellular uptake was minimized under low temperature. In order to evaluate the receptor targeting specificity of **Den-RGD-Angio**, U87MG cells were treated with this nanoprobe in the presence of the low-density lipoprotein receptor-associated protein (RAP), which was utilized as a receptor competitor of LRP receptor, and free c[RGDyK] peptide, which was utilized as a competitor of $\alpha_V\beta_3$ integrin. While the uptake of **Den-RGD-Angio** did not change upon treatment with c[RGDyK], no cellular uptake of this nanoprobe was monitored after the preincubation of RAP

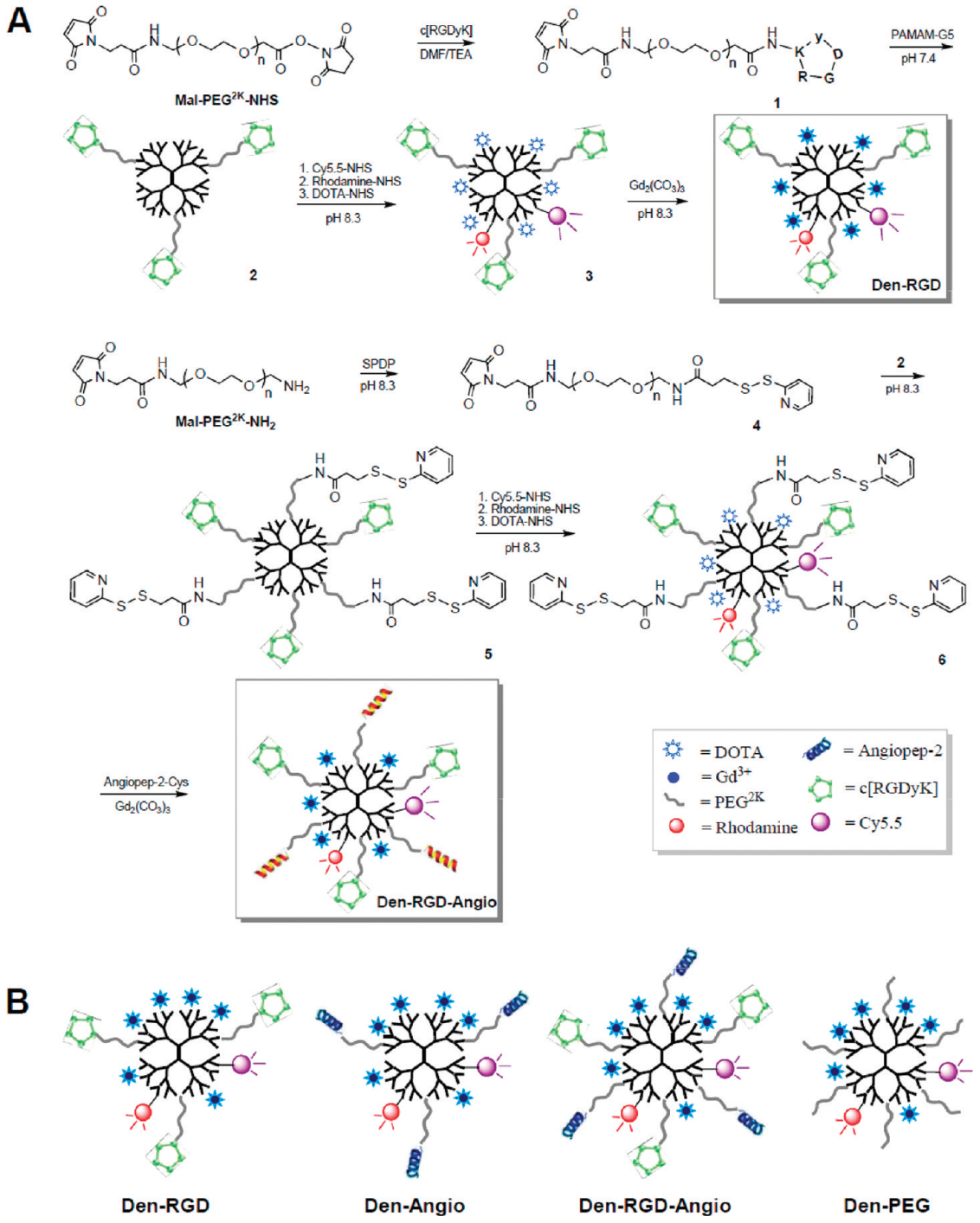

Figure 2. (A) Synthetic steps of nanoprobes Den-RGD and Den-RGD-Angio. (B) Schematics of the targeted and control nanoprobes.

(Figure 3A). The above results indicated that LRP receptor played a predominant role in the cellular uptake of **Den-RGD-Angio**. After 24 h incubation at 37 °C, while **Den-RGD-Angio** distributed in the whole cytoplasm as vesicular structures, **Den-PEG** was sporadically located at the perinuclear areas (Figure 3B). Internalizations of **Den-RGD** and **Den-Angio** were evident, but their uptakes were obviously lower than that of **Den-RGD-Angio**. Interestingly, quite different time-dependent internalization patterns of the nanoprobes were observed by flow cytometry (Figure 3C and Figure S5). **Den-RGD-Angio** and **Den-Angio** showed their fastest uptakes in the first 15 min. The initial uptake rates of **Den-PEG** and **Den-RGD** were much lower than that of **Den-RGD-Angio**; however, a sustained internalization of **Den-RGD** was observed. Average cellular fluorescence intensity was quantified in the order **Den-RGD-Angio** > **Den-Angio** > **Den-RGD** > **Den-PEG** during the whole treatment procedure, and the cellular uptake of **Den-RGD-Angio**

was found to be significantly higher than those of **Den-Angio** and **Den-PEG** ($p < 0.001$, $n = 4$) at 15 min and 1 and 24 h post-treatment (Figure 3D).

***In Vivo* Imaging Studies.** Dynamic T1-weighted MR images showed a prolonged circulation lifetime of **Den-RGD-Angio** because the MR signal enhancement in intracerebral vasculatures such as the superior sagittal sinus and straight sinus lasted for more than 2 h (upper panel of Figure 4A). BBB permeability of **Den-RGD-Angio** was obvious with evidence of platelet-like hyperintense regions (positive contrast) in the cortex at 24 h postinjection (PI). The average MR signal in the cortex increased 7.5% ($n = 4$) compared to its precontrast values at 24 PI. BBB permeability of **Den-RGD-Angio** was further verified by the *in vivo* NIR fluorescence imaging (Figure 4C). The merged X-ray/optical image of an enlarged mouse head clearly indicated the location of this nanoprobe inside the skull that was delineated by X-ray image. In contrast, the intracranial NIR fluorescence of **Den-PEG** remained at the background level during the whole imaging process.

T1-weighted MR imaging demonstrated the feasibility of **Den-RGD-Angio** to visualize the orthotropic U87MG glioblastoma xenograft *in vivo*. A heterogeneous MR signal enhancement in tumor was observed as fast as 10 min PI. The tumor boundary was more evident at 2 h PI, and it correlated well with the H&E stained histological tissue section of the identical brain tissues (lower panel, Figure 4A). Figure 4B shows that the MR signal intensity ratio between the tumor and surrounding normal neurological tissue (T/N ratio) kept increasing after **Den-RGD-Angio** administration and reached its maximum value of 1.52 at 24 h PI.

TABLE 1. Physical Parameters of the Nanoprobes

nanoprobe	d (nm)[a]	PDI[a]	ζ (mV)[a]	Gd %[b]	r_{1p} (mM^{-1} s^{-1})[c]	MW (kDa)[d]
Den-PEG	11.5	0.258	16.7	12.5	7.4 ± 0.4	82
Den-RGD	13.2	0.193	10.4	9.6	7.1 ± 0.3	81
Den-Angio	13.3	0.287	11.6	9.4	6.9 ± 0.4	83
Den-RGD-Angio	15.6	0.224	8.6	9.6	7.1 ± 0.2	91
G5 dendrimer	7.1	0.157	21.5	n.d.	n.d.	30

[a] Diameters (d), polydispersity index (PDI), and zeta potentials (ζ) were measured by dynamic light scattering (DLS).. [b] Gadolinium concentrations (Gd %) were measured by inductively coupled plasma atomic emission spectroscopy (ICP-AES). [c] T1-weighted relaxivities (r_{1p}) were determined on 4.7 T MRI at 25 °C.. [d] Molecular weights (MW) were measured by MALDI-TOF MS.

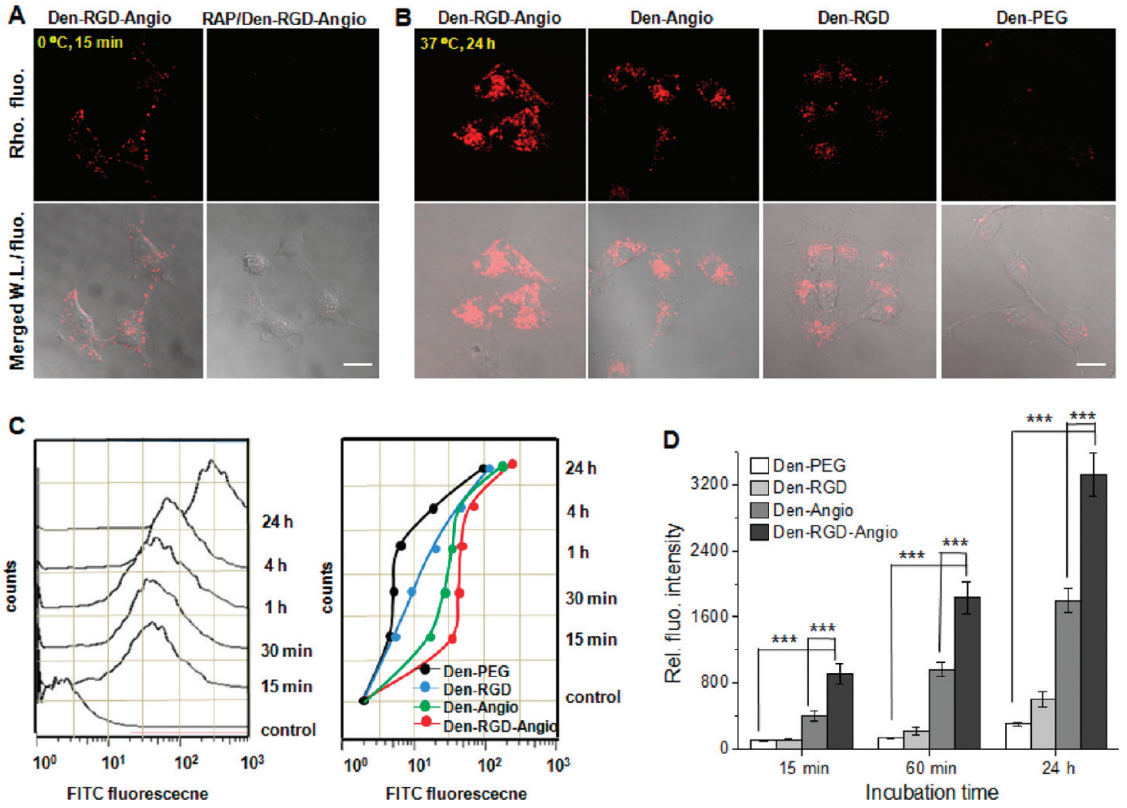

Figure 3. Den-RGD-Angio demonstrated a higher cellular uptake efficacy than the control nanoprobes in U87MG cells. (A) Confocal fluorescence microscopic images of the live cells treated with 1.0 μM Den-RGD-Angio for 15 min or pretreated with 2.0 μM RAP for 30 min followed by the nanoprobe treatment. The above experiments were conducted at 4 °C. Rhodamine fluorescence is displayed in red. (B) Microscopic fluorescence images of the live cells treated with 1.0 μM selected nanoprobe for 24 h at 37 °C. Scale bar: 15 μm. (C) Time-dependent flow cytometries of the cells treated with Den-RGD-Angio (1.0 μM, left panel) and time-dependent cellular fluorescence intensity curves after treatment of nanoprobe (1.0 μM, right panel). (D) Mean cellular fluorescence intensities after nanoprobe treatment for 15 min and 1 and 24 h at 37 °C. The values represent mean ± SD ($n = 4$). (***) $p < 0.001$.

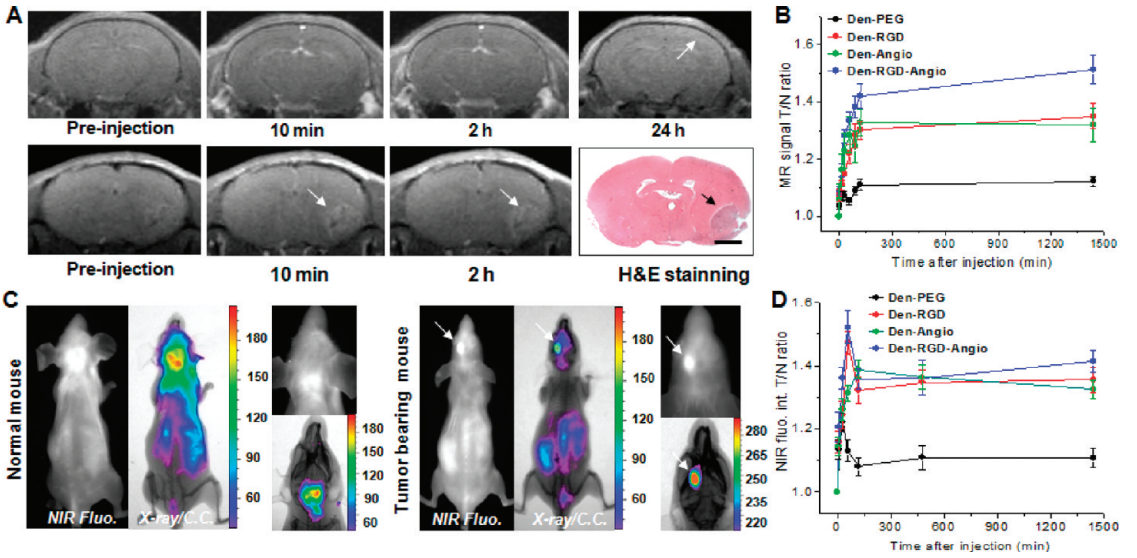

Figure 4. Den-RGD-Angio demonstrated high BBB permeability and T/N ratio *in vivo*. (A) Representative T1-weighted MR images of normal mouse brain (upper panel, arrow points to the cortex) and tumor-bearing brain (lower panel, arrows point to the tumor) before and at selected time PI of Den-RGD-Angio (0.05 mmol/kg [Gd^{3+}], *iv*). Histological H&E staining verified the tumor boundary in MRI (bar, 2.0 mm). (B) *In vivo* time-dependent MR signal associated T/N ratio before and PI of nanoprobe (n = 4). Points present mean values and bars show the maximum and minimum values (data range). (C) Representative NIR fluorescence and X-ray/color coded NIR fluorescence images of the normal mouse (left panel) and brain tumor-bearing mouse (right panel) at 24 h PI of Den-RGD-Angio (5.0 nmol/mouse based on dendrimer). (D) *In vivo* time-dependent NIR fluorescence T/N ratio (n = 3). Points present mean values and bars show the data range.

Den-RGD-Angio also had the highest NIR fluorescence-associated T/N ratio of all the nanoprobes, and its maximal value of 1.49 was measured at 24 h PI (Figure 4C, D).

Biodistribution and *Ex Vivo* Imaging Studies. *Ex vivo* NIR fluorescence images of the excised normal mouse brain unambiguously demonstrated the accumulation of **Den-RGD-Angio** in the cortex of normal brain (Figure 5A). The average NIR fluorescence of **Den-RGD-Angio** in the whole excised brain was measured as 17% (n = 3) higher than that of **Den-PEG** (Figure S6A). Microscopic fluorescent images of normal mouse brain sections showed that **Den-RGD-Angio** and **Den-Angio** penetrated the brain capillaries and located in the cortex parenchyma at 24 h PI (Figure S6B), whereas no detectable intracerebral deliveries of **Den-RGD** and **Den-PEG** were found. **Den-RGD-Angio** also showed the highest T/N ratio in the excised brain bearing U87MG tumor xenograft (Figure 5B), and the data were measured as 5.6 at 24 h PI, which was much higher than the control nanoprobes (n = 3, Figure S6C). The biodistribution data expressed as a percentage of injected dose/gram of tissue (%ID/g) were evaluated in U87MG tumor-bearing mice at 24 h PI of nanoprobes labeled with radioactive ^{125}iodide (Figure 5C). All nanoprobes mainly located in the liver, spleen, and kidney. The intratumoral uptake of **Den-RGD-Angio** (0.36 ± 0.05% ID g^{-1}) was about 1.4, 1.7, and 2.6 times higher than that of **Den-RGD**, **Den-Angio**, and **Den-PEG**, respectively. Figure 5D shows the white light and corresponding radioautographic images of the tumor-bearing brain sections at 24 h PI of the ^{125}I-labeled nanoprobes. The intratumoral delivery of nanoprobes was evident with the high radioactivity (displayed as dark color) shown in the tumor area. **Den-RGD-Angio** gave the highest T/N ratio, which was measured as 1.41 at 24 h PI.

Microscopic Immunofluorescence Imaging Studies. Figure 6A shows the fluorescence microscopic images of tumor-bearing brain sections at 24 h PI of nanoprobe. In contrast to the concentrated distribution of **Den-RGD-Angio** in the entire tumor, **Den-PEG** was only scattered at the tumor boundary, which can be defined by the fluorescence images of nucleus stained by DAPI. The enlarged images indicate that **Den-RGD-Angio** was internalized into the cancer cells and distributed as the vascular structures at the perinucleus areas. The intratumoral deliveries of **Den-RGD** and **Den-Angio** were lower than that of **Den-RGD-Angio** but significantly higher than that of **Den-PEG**. Figure 6B shows the average cellular fluorescence intensities in the tumor and normal cells at 24 h PI of nanoprobe. Compared to **Den-PEG**, the average fluorescence intensities in normal neurological cells increased 1.2, 1.6, and 1.7 (15 slices analyzed from three tumors) times for **Den-RGD**, **Den-Angio**, and **Den-RGD-Angio**, respectively. Remarkably, the average fluorescence intensities of **Den-RGD**, **Den-Angio**, and **Den-RGD-Angio** in brain tumor cells were measured as 2.8, 2.7, and 4.5 times higher than that of **Den-PEG**.

This two-order targeted imaging of **Den-RGD-Angio** was further investigated by microscopic immunofluorescence imaging. First, the targeting specificity of **Den-RGD-Angio** to $\alpha_v\beta_3$ integrin was assessed at 2 and 24 h PI of the nanoprobe. The β_3 integrin was predominately located at the tumor margin with high

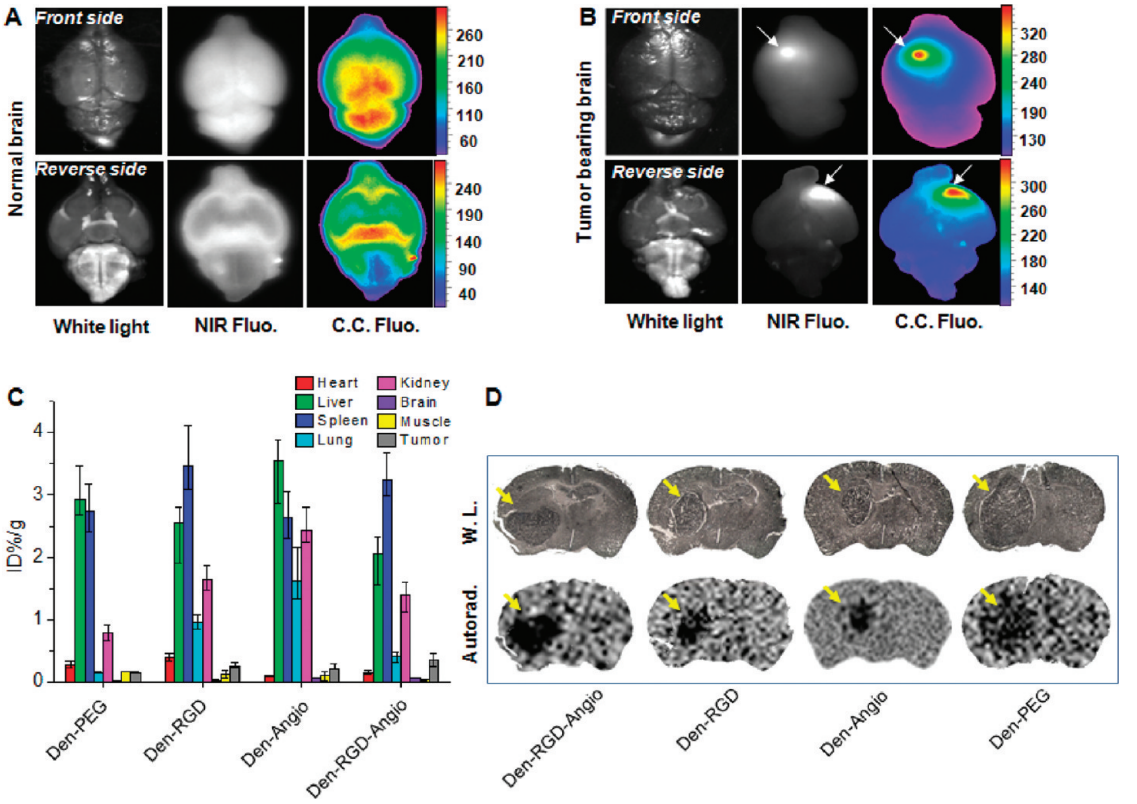

Figure 5. Biodistribution and *ex vivo* imaging studies verified the high T/N ratio of Den-RGD-Angio. Representative white-light, NIR fluorescence, and color-coded fluorescence images of normal mouse brain (A) and tumor-bearing mouse brain (B) at 24 h PI of Den-RGD-Angio. Arrow points to the tumor. (C) Biodistribution of nanoprobe labeled with ^{125}I radioactive isotope (1.8×10^5 Bq/mouse) in tumor-bearing mice ($n = 3$) at 24 h PI. Columns present mean values, and bars present the data range. (D) Representative white-light microscopic images and autoradiographic images of tumor-bearing brain sections at 24 h PI of the radioactive nanoprobe. Arrows point to the tumors.

vasculature density (Figure 6C). The rhodamine fluorescence of **Den-RGD-Angio** co-localized well with the β_3 integrin immunofluorescence at 2 h PI. However, the co-localization coefficient between the β_3 integrin and nanoprobe decreased from 0.74 at 2 h PI to 0.26 (18 slices analyzed from three tumors) at 24 h PI due to the continued uptake of this nanoprobe in the tumor core area (Figure 6D). The targeting specificity of nanoprobe to the LRP receptors was also studied. The LRP receptors are heterogeneously located in the brain tumor, and the co-localization coefficient between LRP receptor and **Den-RGD-Angio** was determined to be as high as 0.86 at 2 h PI (Figure 6D). Interestingly, the immunofluorescence of LRP receptor in the tumor core area disappeared and the co-localization coefficient reduced to 0.07 (18 slices analyzed from three tumors) at 24 PI.

DISCUSSION

Poor BBB permeability of the imaging/therapeutic agents is a bottleneck that limits the successful brain tumor diagnosis and treatment. In proof-of-principle, we put forward a novel two-order targeted nanoprobe to noninvasively image the brain tumor by circumventing BBB *in vivo*. The up-regulated BBB traversing efficacy of this nanoprobe results from (1) multivalent effect that boosts the avidity to the targeted receptor on brain tumor vasculatures. For example, Josephson *et al.* reported that the binding affinity of the nanoparticle modified with 20 c[RGDfK] peptides was 71 times higher compared to that of the free peptide;[37] (2) high local ligand concentration effect that up-regulates the receptor-mediated transcytosis. DeSimone *et al.* reported that the cellular uptake of the PRINT nanoparticle was proportional to the density of the labeled Tf.[38] Therefore, a combination of the multivalent effect and the high local ligand concentration effect can remarkably increase the BBB permeability of nanoprobes.

Higher permeability of tumor vasculature provided a natural selection process to allow the nanoparticles to extravasate into the tumor interstitium but not the normal tissues.[39] However, brain tumor vasculature (BTV) retains some features of the BBB such as tight interendothelial junctions and transendothelial channels.[15] For example, Sarin *et al.* found the upper limit of the pore size in BTV would be less than 20 nm in diameter,[33] which is much smaller than that of extracranial tumors up to 1−5 μm.[39] Furthermore, nanoprobes smaller than 5 nm are also not suitable for brain

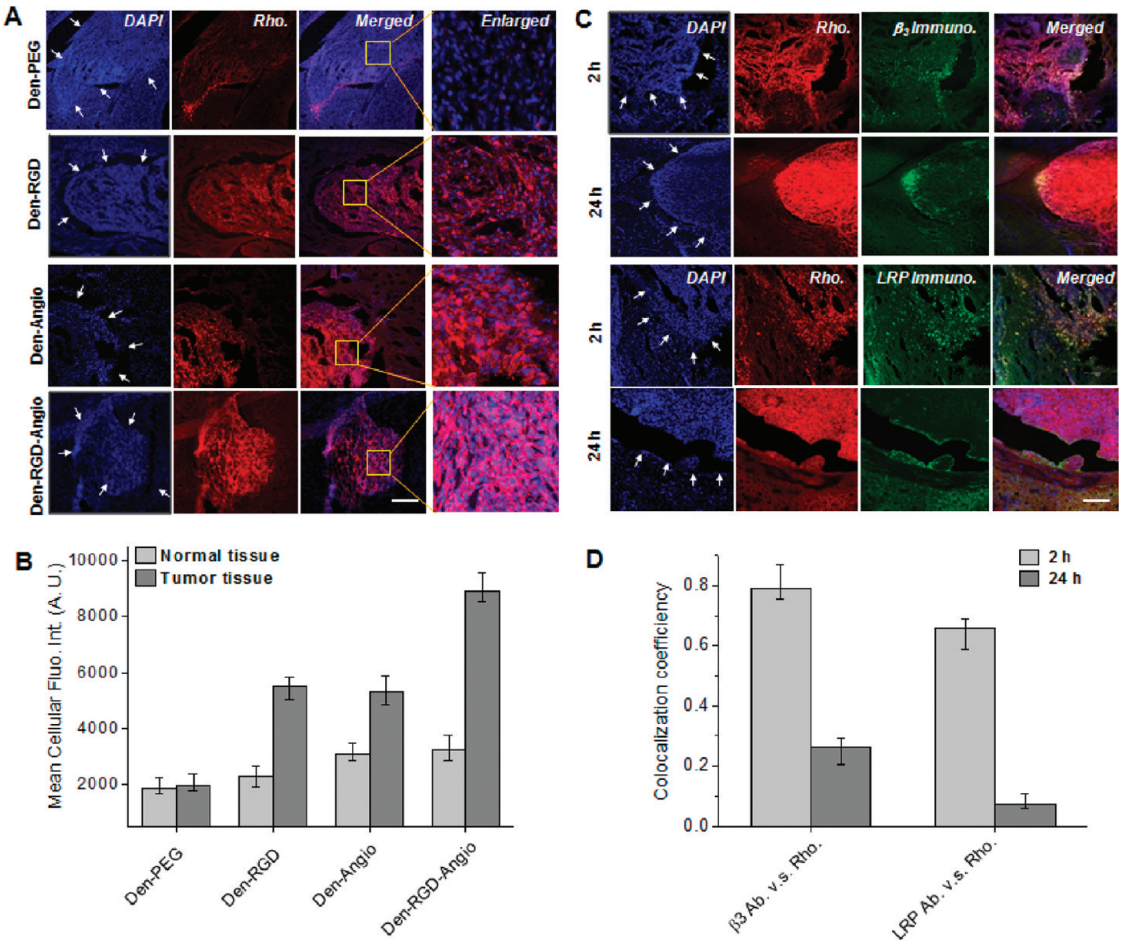

Figure 6. $\alpha_V\beta_3$ integrin and LRP receptor are involved in the two-order targeted imaging strategy. (A) Representative confocal microscopic fluorescence images of tumor-bearing brain sections at 24 h PI of nanoprobe (5.0 nmol/mouse). Rhodamine in the nanoprobe is displayed in red, and the nuclei stained with DAPI are shown in blue. Tumor boundary is indicated by the arrows. Scale bar: 200 μm. (B) Intracellular fluorescence intensity at 24 h PI of the nanoprobe. The data were quantified by normalizing the gross rhodamine fluorescence with the number of nuclei in the indicated areas. Columns present mean values, and bars present the data range (15 randomly selected images analyzed from three tumors after a nanoprobe injection). (C) Representative microscopic fluorescence images of tissue sections immunohistologically stained with β_3 integrin antibody (upper panel) and LRP antibody (lower panel) at 2 and 24 h PI of Den-RGD-Angio. The immunofluorescence is displayed in green. Scale bar: 200 μm. (D) Co-localization coefficients between the nanoprobe fluorescence and the immunofluorescence in the tumor at 2 and 24 h PI of Den-RGD-Angio (18 randomly selected images analyzed from three tumors after a nanoprobe injection).

tumor imaging because their fast excretion *via* renal filtration results in their transient residence in the blood pool.[40] In this work, the diameters of the nanoprobes are in a range 11−16 nm, which are small enough to traverse BTV but big enough to achieve a prolonged circulation lifetime. The reduced cytotoxicity of the nanoprobes compared to the unmodified dendrimer can be explained by their lower positive charges, which reduce the nonspecific accumulation of nanoprobe in normal tissues.[41] However, the residue positive charge of the nanoprobes could potentially facilitate their intratumoral uptake *via* the electrostatic interaction between the cationic nanoprobe and the negatively charged sulfated proteoglycans overexpressed on the cancer cells.[42] The high sensitivity of NIR fluorescence imaging can compensate the inherent shortage of MRI by using multimodal nanoprobes, and it is promising to generate the images with high spatial resolution as well as sensitivity. Due to the numerous MR chelators labeled on the nanoprobe, the overall relaxivity of the nanoprobe can be as high as 355 mM^{-1} s^{-1}/nanoprobe, which benefits the generation of detectable MR signals even when nanoprobe concentration is low in brain tissues.

In vitro competition studies clearly indicated the dominant role of the LRP receptor in the cellular uptake of **Den-RGD-Angio**. Actually, the maximum cellular uptake velocity of **Den-RGD-Angio** measured in the beginning of treatment can be explained by the overwhelming ligand/receptor association, which is much faster than active internalization. The highest cellular uptake rate of **Den-RGD-Angio** in the whole incubation period presumably results from a synergistic receptor targeting effect of angiopep-2 and c[RGDyK] peptides.

BBB permeability of **Den-RGD-Angio** was unambiguously verified by *in vivo* MR/optical imaging, *ex vivo* optical imaging, and microscopic imaging studies. The role of LRP receptor mediated transcytosis in intracerebral delivery is obvious because MR/NIR fluorescence signal enhancements in the cortex were observed only after the injection of nanoprobes modified with angiopep-2 ligand. Interestingly, even angiopep-2 densities on **Den-RGD-Angio** and **Den-Angio** were the same, and **Den-RGD-Angio** showed a higher BBB traverse efficiency compared to **Den-Angio**. Milner *et al* reported the presence of $\alpha_V\beta_3$ integrin in the BCECs.[43] The synergistic targeting effect of **Den-RGD-Angio** found in cell culture studies may also increase its local concentration in BCECs, which further accelerates its BBB traverse efficiency. Due to the high tissue penetration capability of NIR fluorescence, the intracerebral delivery of nanoprobes was detected by NIR optical imaging as early as 2 h PI, which provided a convenient and sensitive way to dynamically track the intracerebral delivery of nanoprobes.

Both MR and optical imaging demonstrated the intratumoral delivery of all four nanoprobes *in vivo*. Due to the EPR effect, all nanoprobes can enter the tumor by extravasating the impaired BBB. However, compared to the controls, **Den-RGD-Angio** not only offered the highest T/N ratio but also precisely delineated the tumor boundary. The perfect tumor boundary correlation between the *in vivo* MR image and the *ex vivo* histological images indicates the feasibility of this nanoprobe to surgically locate the brain tumor. Recently, Zhang *et al*. reported an iron oxide nanoparticle based T2-weight MR probe modified with chlorotoxin as the targeting ligand.[44] Even though this nanoprobe successfully visualized the transgenic ND2:SmoA1 brain tumor *in vivo*, the neoplastic tissue cannot be precisely defined until 48 h PI due to the slow extravasation rate of the nanoprobe. Furthermore, the "negative contrast" signal induced by the iron oxide particles may mislead the clinical diagnosis because endogenous tissues such as necrosis, calcification, hemorrhage, or metal deposition are also present as "hyphointense areas" in MRI.[45] Therefore, our nanoprobe with fast intratumoral delivery rate and "positive" signal enhancement in neoplastic tissues is more desirable to the radiologist. Furthermore, due to the extremely high T/N ratio of **Den-RGD-Angio** in the *ex vivo* optical imaging studies, this nanoprobe holds promise in real-time optical imaging guided surgery to completely remove neoplastic tissues with minimized impairment of the surrounding normal neurological tissues.

As indicated in the microscopic immunofluorescence studies, high co-localization coefficients between **Den-RGD-Angio** and the LRP receptor as well as β_3 integrin at 2 h PI indicated the involvement of both receptors in the targeted delivery of nanoprobes. Additionally, in contrast to the location of **Den-PEG** at the tumor periphery, **Den-RGD-Angio** was distributed in the whole tumor area and internalized in the cytoplasm. The above experimental results support the assumed two-order targeted imaging strategy. At 24 h PI, remarkably reduced co-localization coefficients may be interpreted by the "receptor occupation effect",[46] in which the receptors on cancer cells are occupied by the nanoprobe and hard to immunostain by corresponding antibodies. Compared to the **Den-PEG**, the average cellular fluorescence intensities of **Den-RGD-Angio** and **Den-Angio** in normal brain tissues increased to 67−75%, which is solid evidence for the LRP-mediated transcytosis *in vivo*. Overall, the combination of the EPR effect, the up-regulated BBB permeability, and the two-order targeting strategy contributes to the high T/N ratio of **Den-RGD-Angio**.

CONCLUSION

Overall, this work developed a novel two-order targeted imaging strategy that successfully visualized orthotropic brain tumor xenografts with high sensitivity and target to background signal ratio *in vivo*. This multimodal nanoprobe not only demonstrated the feasibility to preoperatively localize brain tumors by both MRI and optical imaging but also provided a potential solution to delineate the malignant tumor with uncompromised BBB. Additionally, due to its extraordinarily high T/N ratio shown under *ex vivo* conditions, this nanoprobe holds promise in NIR optical image-guided brain tumor resection during surgery.

MATERIALS AND METHODS

Materials. All chemicals were analytical grade from Aladdin Reagent (Shanghai, China) unless otherwise specified. PAMAM G5 dendrimer (77.35 mg/mL in MeOH) was purchased from Dendritech Inc. (Midland, MI, USA). Rhodamine-NHS, Cy5.5-NHS, and SPDP were from Thermofisher Scientific (New York, USA). Fetal bovine serum, penicillin, streptomycin, Alexa Fluo 488, and horseradish peroxidase (HRP)-labeled goat anti-rabbit secondary antibodies were from Invitrogen (Carlsbad, CA, USA). Rabbit anti-mouse/human β-actin, β_3 integrin, and LRP-1 primary antibodies were from Epitomics (Burlingame, CA, USA). Malemide-PEG^{2k}-NHS and PEG^{2K}-NHS were from JenKem Technology (Beijing, China). DOTA-NHS was prepared according to a previous report.[47] $Gd_2(CO_3)_3$, DAPI, Bolton-Hunter reagent, and MTT were purchased from Sigma-Aldrich (St. Louis, MO, USA). Isoflurane was from Baxter Healthcare Corporation (New Providence, NJ, USA).

Western Blot Studies. Approximately 3×10^6 cells at 80% confluence were homogenized with lysis buffer containing protease inhibitors. Then 80 μg of total protein determined by a modified Lowry assay (Bio-Rad) was resolved on 7% SDS-PAGE. The gels were transferred to polyvinylidenedifluoride membranes, blocked, cut, and incubated with β-actin (1:50 000) or β_3 integrin (1:1000) or LRP-1 (1:20 000) primary antibodies. The membrane was incubated with HRP-labeled goat anti-rabbit

secondary antibody (1:2000) and visualized by using the Supersignal WestPico chemiluminescent substrate kit (Pierce Biotechnology, Rockford, IL, USA).

Cell Culture Studies. U87MG, PC3, MDA-MB-231, and BCECs (ATCC) were cultured as recommended by the supplier.

Confocal Fluorescence Microscopic Imaging. Fluorescence microscopic images were collected on a Zeiss LSM 510 META confocal laser scanning microscope (Carl Zeiss, Germany) by using a 40× oil immersion lens. DAPI was excited with a 405 nm laser, and the emission was detected with a photomultiplier by a 420−480 nm band-pass filter. Alexa Flour 488 was excited with a 495 nm laser, and emission was detected by a second photomultiplier using a 505−550 nm band-pass filter. Rhodamine was excited with a 543 nm laser, and the emission was detected by a third photomultiplier using a 560 nm band-pass filter.

Flow Cytometry. U87MG cells with 80% confluence were treated with 1.0 μM nanoprobes in which the rhodamine was replaced by fluorescein. At the end of incubation, the cells were washed, centrifuged, fixed, and analyzed by BD FACSAria (BD Biosciences, USA) equipped with a 488 nm Ar ion laser.

Tumor Implantation. All animal experiments were carried out in accordance with guidelines approved by the ethics committee of Fudan University, Shanghai, China. U87MG cells (5.0×10^5) were inoculated into the right striatum (1.8 mm lateral, 0.6 mm anterior to the bregma, and 3.0 mm of depth) of male Balb/c nude mice by using a stereotactic fixation device with mouse adaptor. The intracranial tumors with a diameter of 0.5−1.0 mm were ready for imaging after inoculation for 14−18 days.

***In Vivo* MRI Studies.** *In vivo* MR imaging was carried out on a Biospec 47/30 MRI scanner (Bruker Inc., Billerica, MA). The mice were anesthetized with isoflurane and placed into a mice bed. Mouse respiration was continuously monitored by Biotrig software. A volume coil was used for RF transmission and a quadrature surface coil for signal detection. Dynamic T1-weighted images of the brain were collected before and after bolus administration of nanoprobe with a dose of 0.05 mmol/kg [Gd^{3+}] in a 0.25 mL of PBS *via iv*. Coronal images of the brain sections with 1.0 mm thickness were acquired with a spin−echo pulse sequence [field of view (FOV): 2 cm × 2 cm, matrix size: 128 × 128, TR = 300 ms, TE = 11 ms, and number of average = 8]. The intensity enhancement (IE) of region of interest at time point t is expressed by $IE = (RI(t) - RI(0))/RI(0) \times 100\%$, where $RI(t)$ and $RI(0)$ correspond to the normalized signal intensities measured at time point t and preinjection.

***In Vivo* and *ex Vivo* Optical Imaging Studies.** Optical images were acquired on a Kodak Multispectral Imaging System equipped with a 750 nm excitation filter and a 800 nm emission band-pass filter set. All X-ray images were acquired by using a 0.2 s exposure time, and NIR fluorescence images were acquired using a 0.5 s exposure time (FOV = 6.4 or 12.8 cm; f/stop, 4; bin, high resolution). The fluorescence intensities were quantified by ImageJ software (NIH).

Biodistribution. Nanoprobes were radiolabeled with ^{125}I isotope by using Bolton-Hunter reagent (Pierce Biotechnology, USA). U87MG tumor-bearing mice were randomly divided into four groups and injected with [^{125}I]-labeled nanoprobe (3.0×10^5 Bq/mouse) *via iv*. The mice were sacrificed at 24 h PI and perfused with saline. Selected organs were excised and weighed, and the radioactivity was counted with an automatic γ-counter. The biodistribution data are presented as percentage of the injected dose per gram.

Autoradiography Studies. After biodistribution studies, mouse brains were excised and cryo-sectioned with a thickness of 20 μm. The autoradiogram images were collected by a Cyclone Pulse Storage Phosphor system (Perkin-Elmer, USA) with an exposure time of 24 h. The white-light pictures of these brain sections were taken by a Leica MZ75 (Leica Inc., Germany) high-performance stereomicroscope equipped with 2.5× plano objective.

Histological and Immunohistological Staining. Tumor-bearing brains were fixed, dehydrated, and sectioned at least 15 sections per brain with a thickness of 20 μm. The sections from each brain were divided into three groups. Group one were stained with hematoxylin and eosin (H&E); group two were stained with β_3 integrin primary antibody followed the fluorophore-labeled secondary antibody and DAPI; group three were stained by LRP-1 primary antibody followed the secondary antibody and DAPI.

Statistical Analysis. Values are mean ± SD when the sample number is above 3 ($n > 3$). Statistical differences were evaluated with two-tailed corrected Student's t test (SPSS, IBM); $p < 0.05$ was considered significant. Values are presented as mean and data range (from minimum value to maximum value) when the sample number is 3 ($n = 3$).

Acknowledgment. This work was supported by the National Basic Research Program of China (973 Program, 2011CB910404), the National Natural Science Foundation of China (Nos. 81171384, 20975027, 20921004, 20820102035), Shenzhen Bio-industry Development Fund-Basic Research Program (JC201005280607A), and Program for New Century Excellent Talents in University Award (NCET-08-0131). We are grateful for the helpful discussion with Prof. X. Y. Feng and Prof. C. Jiang.

Supporting Information Available: Details of nanoprobe synthesis, characterization, *in vitro* cytotoxicity studies, Figures S1−S6, and NMR and MS spectra. This material is available free of charge *via* the Internet at http://pubs.acs.org.

REFERENCES AND NOTES

1. Wen, P. Y.; Kesari, S. Malignant Gliomas in Adults. *N. Engl. J. Med.* **2008**, *359*, 492–507.
2. Huse, J. T.; Holland, E. C. Targeting Brain Cancer: Advances in the Molecular Pathology of Malignant Glioma and Medulloblastoma. *Nat. Rev. Cancer* **2010**, *10*, 319–331.
3. Laws, E. R.; Parney, I. F.; Huang, W.; Anderson, F.; Morris, A. M.; Asher, A.; Lillehei, K. O.; Bernstein, M.; Brem, H.; Sloan, A.; *et al*. Survival Following Surgery and Prognostic Factors for Recently Diagnosed Malignant Glioma: Data from the Glioma Outcomes Project. *J. Neurosurg.* **2003**, *99*, 467–473.
4. Donahue, M. J.; Blakeley, J. O.; Zhou, J.; Pomper, M. G.; Laterra, J.; van Zijl, P. C. Evaluation of Human Brain Tumor Heterogeneity Using Multiple T1-Based MRI Signal Weighting Approaches. *Magn. Reson. Med.* **2008**, *59*, 336–344.
5. Zhou, J.; Tryggestad, E.; Wen, Z.; Lal, B.; Zhou, T.; Grossman, R.; Wang, S.; Yan, K.; Fu, D. X.; Ford, E.; *et al*. Differentiation between Glioma and Radiation Necrosis Using Molecular Magnetic Resonance Imaging of Endogenous Proteins and Peptides. *Nat. Med.* **2011**, *17*, 130–134.
6. Weber, M. A.; Giesel, F. L.; Stieltjes, B. MRI for Identification of Progression in Brain Tumors: from Morphology to Function. *Expert Rev. Neurother.* **2008**, *8*, 1507–1525.
7. Giesel, F. L.; Mehndiratta, A.; Essig, M. High-Relaxivity Contrast-Enhanced Magnetic Resonance Neuroimaging: A Review. *Eur. Radiol.* **2010**, *20*, 2461–2474.
8. Scott, J. N.; Brasher, P. M.; Sevick, R. J.; Rewcastle, N. B.; Forsyth, P. A. How Often Are Nonenhancing Supratentorial Gliomas Malignant? A Population Study. *Neurology* **2002**, *59*, 947–949.
9. Whitesides, G. M. The 'Right' Size in Nanobiotechnology. *Nat. Biotechnol.* **2003**, *21*, 1161–1165.
10. Maeda, H. Tumor-Selective Delivery of Macromolecular Drugs *via* the EPR Effect: Background and Future Prospects. *Bioconjugate Chem.* **2010**, *21*, 797–802.
11. Torchilin, V. Tumor Delivery of Macromolecular Drugs Based on the EPR Effect. *Adv. Drug Delivery Rev.* **2011**, *63*, 131–135.
12. Hong, S.; Leroueil, P. R.; Majoros, I. J.; Orr, B. G.; Baker, J. R., Jr.; Banaszak Holl, M. M. The Binding Avidity of A Nanoparticle-Based Multivalent Targeted Drug Delivery Platform. *Chem. Biol.* **2007**, *14*, 107–115.
13. Janib, S. M.; Moses, A. S.; MacKay, J. A. Imaging and Drug Delivery Using Theranostic Nanoparticles. *Adv. Drug. Delivery Rev.* **2010**, *62*, 1052–1063.
14. Li, C.; Xia, J.; Wei, X.; Yan, H.; Si, Z.; Ju, S. pH-Activatable Near-Infrared Fluorescence Nanoprobe Imaging Tumors by Sensing the Acidic Microenvironment. *Adv. Funct. Mater.* **2010**, *20*, 2222–2230.

15. Black, K. L.; Ningaraj, N. S. Modulation of Brain Tumor Capillaries for Enhanced Drug Delivery Selectively to Brain Tumor. *Cancer Control* **2004**, *11*, 165–173.
16. Shi, N.; Boado, R. J.; Pardridge, W. M. Receptor-Mediated Gene Targeting to Tissues *in Vivo* Following Intravenous Administration of Pegylated Immunoliposomes. *Pharm. Res.* **2001**, *18*, 1091–1095.
17. Huang, R.; Ke, W.; Liu, Y.; Jiang, C.; Pei, Y. The Use of Lactoferrin as a Ligand for Targeting the Polyamidoamine-Based Gene Delivery System to the Brain. *Biomaterials* **2008**, *29*, 238–246.
18. Liu, Y.; Huang, R.; Han, L.; Ke, W.; Shao, K.; Ye, L.; Lou, J.; Jiang, C. Brain-Targeting Gene Delivery and Cellular Internalization Mechanisms for Modified Rabies Virus Glycoprotein RVG29 Nanoparticles. *Biomaterials* **2009**, *30*, 4195–4202.
19. Zhan, C.; Li, B.; Hu, L.; Wei, X.; Feng, L.; Fu, W.; Lu, W. Micelle-Based Brain-Targeted Drug Delivery Enabled by a Nicotine Acetylcholine Receptor Ligand. *Angew. Chem., Int. Ed.* **2011**, *50*, 5482–5485.
20. He, H.; Li, Y.; Jia, X. R.; Du, J.; Ying, X.; Lu, W. L.; Lou, J. N.; Wei, Y. PEGylated Poly(amidoamine) Dendrimer-Based Dual-Targeting Carrier for Treating Brain Tumors. *Biomaterials* **2011**, *32*, 478–487.
21. Brooks, P. C.; Clark, R. A.; Cheresh, D. A. Requirement of Vascular Integrin Alpha v Beta 3 for Angiogenesis. *Science* **1994**, *264*, 569–571.
22. Hynes, R. O. Integrins: Bidirectional, Allosteric Signaling Machines. *Cell* **2002**, *110*, 673–687.
23. Schottelius, M.; Laufer, B.; Kessler, H.; Wester, H. J. Ligands for Mapping Alphavbeta3-Integrin Expression *in Vivo*. *Acc. Chem. Res.* **2009**, *42*, 969–980.
24. Shibata, M.; Yamada, S.; Kumar, S. R.; Calero, M.; Bading, J.; Frangione, B.; Holtzman, D. M.; Miller, C. A.; Strickland, D. K.; Ghiso, J.; *et al*. Clearance of Alzheimer's Amyloid-ss(1−40) Peptide from Brain by LDL Receptor-Related Protein-1 at the Blood-Brain Barrier. *J. Clin. Invest.* **2000**, *106*, 1489–1499.
25. Ito, S.; Ohtsuki, S.; Terasaki, T. Functional Characterization of the Brain-to-Blood Efflux Clearance of Human Amyloid-Beta Peptide (1−40) across the Rat Blood-Brain Barrier. *Neurosci. Res.* **2006**, *56*, 246–252.
26. Demeule, M.; Regina, A.; Che, C.; Poirier, J.; Nguyen, T.; Gabathuler, R.; Castaigne, J. P.; Beliveau, R. Identification and Design of Peptides as a New Drug Delivery System for the Brain. *J. Pharmacol. Exp. Ther.* **2008**, *324*, 1064–1072.
27. Mazza, M.; Uchegbu, I. F.; Schatzlein, A. G. Cancer and the Blood-Brain Barrier: 'Trojan Horses' for Courses?. *Br. J. Pharmacol.* **2008**, *155*, 149–151.
28. Maletinska, L.; Blakely, E. A.; Bjornstad, K. A.; Deen, D. F.; Knoff, L. J.; Forte, T. M. Human Glioblastoma Cell Lines: Levels of Low-Density Lipoprotein Receptor and Low-Density Lipoprotein Receptor-Related Protein. *Cancer Res.* **2000**, *60*, 2300–2303.
29. Abbott, N. J.; Patabendige, A. A.; Dolman, D. E.; Yusof, S. R.; Begley, D. J. Structure and Function of the Blood-Brain Barrier. *Neurobiol. Dis.* **2010**, *37*, 13–25.
30. Newton, H. B. Advances in Strategies to Improve Drug Delivery to Brain Tumors. *Expert Rev. Neurother.* **2006**, *6*, 1495–1509.
31. Deeken, J. F.; Loscher, W. The Blood-Brain Barrier and Cancer: Transporters, Treatment, and Trojan Horses. *Clin. Cancer Res.* **2007**, *13*, 1663–1674.
32. Barrett, T.; Ravizzini, G.; Choyke, P. L.; Kobayashi, H. Dendrimers in Medical Nanotechnology. *IEEE. Eng. Med. Biol. Mag.* **2009**, *28*, 12–22.
33. Sarin, H.; Kanevsky, A. S.; Wu, H.; Brimacombe, K. R.; Fung, S. H.; Sousa, A. A.; Auh, S.; Wilson, C. M.; Sharma, K.; Aronova, M. A.; *et al*. Effective Transvascular Delivery of Nanoparticles across the Blood-Brain Tumor Barrier into Malignant Glioma Cells. *J. Transl. Med.* **2008**, *6*, 80.
34. He, X.; Gao, J.; Gambhir, S. S.; Cheng, Z. Near-Infrared Fluorescent Nanoprobes for Cancer Molecular Imaging: Status and Challenges. *Trends Mol. Med.* **2010**, *16*, 574–583.
35. Li, C.; Li, Y. X.; Law, G. L.; Man, K.; Wong, W. T.; Lei, H. Fast Water-Exchange Gd^{3+}-(DO3A-Like) Complex Functionalized with Aza-15-Crown-5 Showing Prolonged Residence Lifetime *in Vivo*. *Bioconjugate Chem.* **2006**, *17*, 571–574.
36. Yan, H.; Wang, J.; Yi, P.; Lei, H.; Zhan, C.; Xie, C.; Feng, L.; Qian, J.; Zhu, J.; Lu, W.; *et al*. Imaging Brain Tumor by Dendrimer-Based Optical/Paramagnetic Nanoprobe across the Blood-Brain Barrier. *Chem. Commun. (Cambridge, U.K.)* **2011**, *47*, 8130–8132.
37. Montet, X.; Funovics, M.; Montet-Abou, K.; Weissleder, R.; Josephson, L. Multivalent Effects of RGD Peptides Obtained by Nanoparticle Display. *J. Med. Chem.* **2006**, *49*, 6087–6093.
38. Wang, J.; Tian, S.; Petros, R. A.; Napier, M. E.; Desimone, J. M. The Complex Role of Multivalency in Nanoparticles Targeting the Transferrin Receptor for Cancer Therapies. *J. Am. Chem. Soc.* **2010**, *132*, 11306–11313.
39. Carmeliet, P.; Jain, R. K. Angiogenesis in Cancer and Other Diseases. *Nature* **2000**, *407*, 249–257.
40. Choi, H. S.; Liu, W.; Misra, P.; Tanaka, E.; Zimmer, J. P.; Itty Ipe, B.; Bawendi, M. G.; Frangioni, J. V. Renal Clearance of Quantum Dots. *Nat. Biotechnol.* **2007**, *25*, 1165–1170.
41. Veronese, F. M.; Pasut, G. PEGylation, Successful Approach to Drug Delivery. *Drug Discovery Today* **2005**, *10*, 1451–1458.
42. Li, C.; Wildes, F.; Winnard, P., Jr.; Artemov, D.; Penet, M. F.; Bhujwalla, Z. M. Conjugation of Poly-L-Lysine to Bacterial Cytosine Deaminase Improves the Efficacy of Enzyme/Prodrug Cancer Therapy. *J. Med. Chem.* **2008**, *51*, 3572–3582.
43. Wang, J.; Milner, R. Fibronectin Promotes Brain Capillary Endothelial Cell Survival and Proliferation through Alpha5-beta1 and Alphavbeta3 Integrins *via* MAP Kinase Signalling. *J. Neurochem.* **2006**, *96*, 148–159.
44. Veiseh, O.; Sun, C.; Fang, C.; Bhattarai, N.; Gunn, J.; Kievit, F.; Du, K.; Pullar, B.; Lee, D.; Ellenbogen, R. G.; *et al*. Specific Targeting of Brain Tumors with An Optical/Magnetic Resonance Imaging Nanoprobe across the Blood-Brain Barrier. *Cancer Res.* **2009**, *69*, 6200–6207.
45. Corot, C.; Robert, P.; Idee, J. M.; Port, M. Recent Advances in Iron Oxide Nanocrystal Technology for Medical Imaging. *Adv. Drug Delivery Rev.* **2006**, *58*, 1471–1504.
46. Tallarida, R. J.; Raffa, R. B. The Application of Drug Dose Equivalence in the Quantitative Analysis of Receptor Occupation and Drug Combinations. *Pharmacol. Ther.* **2010**, *127*, 165–174.
47. Li, C.; Winnard, P.; Bhujwalla, Z. M. Facile Synthesis of 1-(Acetic Acid)-4,7,10-Tris(tert-Butoxycarbonylmethyl)-1,4,7,10-Tetraaza-Cyclododecane: A Reactive Precursor Chelating Agent. *Tetrahedron Lett.* **2009**, *50*, 2929–2931.